Advanced Composites and Hybrid Materials (2026) 9:407
https://doi.org/10.1007/s42114-026-01957-7

RESEARCH

Semi-reversible thermochromism in polydiacetylene–PDMS hybrid structures

Inwoong Heo[1] · Seung Soo Shin[1] · Binglun Tu[1] · Boyoung Yoon[1] · Jong-Man Kim[2] · Bum Jun Park[1]

Received: 7 February 2026 / Revised: 2 June 2026 / Accepted: 1 July 2026
© The Author(s) 2026

Abstract
Thermochromic materials that change color in response to temperature have been extensively explored in point-of-use temperature indicators, smart textiles, energy-saving coatings and biomedical monitoring devices. Polydiacetylene (PDA) undergoes a thermally induced blue-to-red transition that is typically irreversible, limiting its use in temperature-responsive sensing. Here, we examine the origin of semi-reversible thermochromism in PDA–PDMS hybrid structures by comparing four architectures: core–shell PDA@PDMS particles, nested-PDAs|PDMS particles, PDA/PDMS composites, and PDA|PDMS laminates. The observed reversibility arises from the melting of residual unpolymerized 10,12-pentacosadiynoic acid (PCDA), its migration into the PDMS matrix, and UV-induced formation of new PDA domains. Systems containing larger PCDA reservoirs show clearer semi-reversible behavior, whereas limited PCDA content results in weak or negligible recovery. Laminate experiments further reveal that PDMS thickness and UV polymerization time influence thermochromic kinetics through their effects on heat transport and PCDA availability. These results clarify the mechanism of semi-reversible thermochromism in PDA-based materials and offer practical considerations for designing thermally responsive PDA systems.

Keywords Polydiacetylene (PDA) · Thermochromism · PDA–PDMS hybrid structures · Reversibility

1 Introduction

Thermochromic materials—solids or liquids that change color in response to temperature—have drawn significant attention for applications ranging from point-of-use temperature indicators and smart textiles to energy-saving coatings and biomedical monitoring devices [1–5]. Their appeal lies in the ability to deliver simple, real-time visual readouts of environmental or process conditions without complex instrumentation. To transition these materials into robust technologies, several performance requirements are generally considered important, including high sensitivity, fatigue resistance, environmental stability, and controlled reversibility with predictable hysteresis over repeated thermal cycles. Unlike fully reversible systems that erase thermal history after cooling, semi-reversible thermochromic materials can retain partial memory of prior thermal exposure while still preserving limited recoverability, making them attractive for thermal-history sensing and programmable colorimetric response systems.

Polydiacetylene (PDA) is a prototypical thermochromic polymer formed by UV-initiated topochemical polymerization of self-assembled diacetylene (DA) monomers such as 10,12-pentacosadiynoic acid (PCDA) [6–11]. Upon 254 nm UV irradiation at ambient conditions, adjacent DA groups arranged in an ordered assembly undergo 1,4-addition polymerization, resulting in the formation of an extended ene–yne conjugated backbone [12, 13]. The resulting conjugated structure typically exhibits an intense blue chromatic phase that undergoes a blue-to-red transition and fluorescence emission upon various external stimuli (e.g., heat, pH, mechanical stress, solvent exposure, and biomolecular

Inwoong Heo, Seung Soo Shin and Binglun Tu contributed equally to this work.

✉ Jong-Man Kim
jmk@hanyang.ac.kr

✉ Bum Jun Park
bjpark@khu.ac.kr

[1] Department of Chemical Engineering (BK21 FOUR Integrated Engineering Program), Kyung Hee University, Yongin 17104, South Korea

[2] Department of Chemical Engineering, Hanyang University, Seoul 04763, South Korea

Published online: 06 July 2026

interactions), driven by conformational rearrangement and partial disruption of π-conjugation (Fig. 1a) [14–25]. Owing to their strong chromatic response and molecular-level sensitivity, PDA-based materials have been widely explored in vesicles, nanoparticles, nanotubes, and thin films, as versatile platforms for stimuli-responsive sensing [26–29]. Nevertheless, many PDA-based sensing studies have primarily focused on ensemble-level responses, particularly in dispersed or solution-phase systems. As a result, direct observation of localized structural changes and spatially resolved chromatic behavior remains limited.

In recent years, our group has explored particle-based PDA architectures to overcome these limitations. Such systems enable single-entity measurements, precise spatial interrogation, and mechanistic analysis of chromatic transitions. For example, we demonstrated that individual PDA

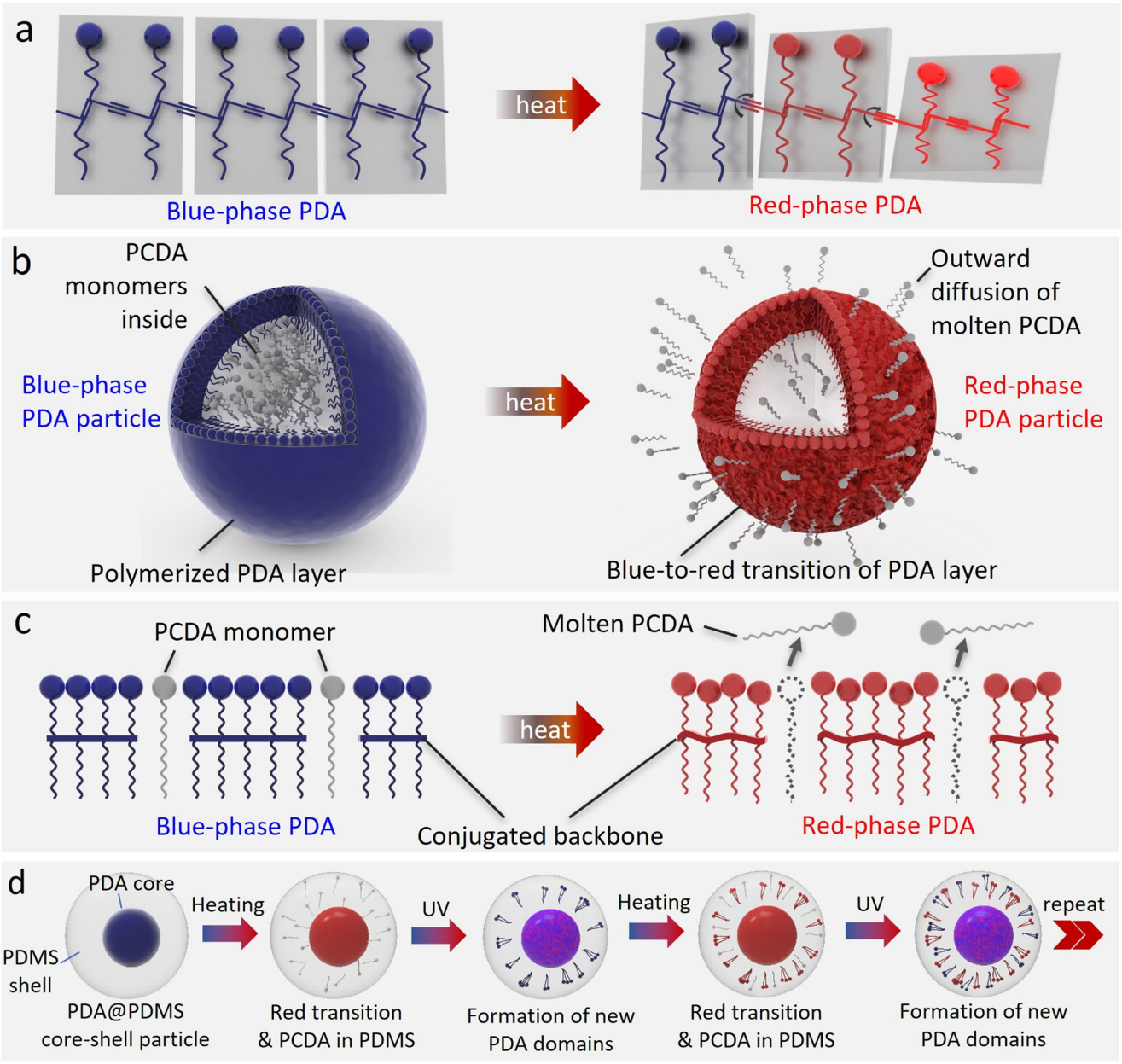


Fig. 1 Schematic illustration of thermochromic transition and PCDA migration in PDA-based systems. **a** Molecular model showing the heat-induced conformational change of the conjugated PDA backbone responsible for the blue-to-red color transition. **b** Structural schematic of a PDA microparticle depicting the outward diffusion of molten PCDA and the blue-to-red transition of the PDA layer upon heating. **c** Illustration of the molecular mechanism for molten PCDA diffusion leading to the formation of red-phase PDA. **d** Cyclic process for a core–shell PDA@PDMS particle: heating causes the red transition and PCDA migration into the PDMS matrix, while subsequent UV irradiation induces the formation of new blue-phase PDA domains, enabling semi-reversible thermochromism upon repeated cycles. All schematics are not drawn to scale

microparticles can function as mechanofluorescent probes reporting flow-induced stress [30]. Micrometer-scale PDA particles, manipulated at oil–water interfaces using optical tweezers [31–33], revealed solvent-dependent dissolution of residual PCDA and Laplace-pressure-driven deformation as key steps underlying solvatochromism [34]. PDA–alginate core–shell particles fabricated via gas-shearing microfluidics have shown controlled solvatochromism in response to polar solvents [35], while microfluidically produced PDA–PDMS core–shell particles exhibited semi-reversible solvatochromism toward apolar solvents, enabling discrimination between closely related solvents such as chloroform and dichloromethane [36]. A consistent feature across these particle systems is that UV polymerization primarily occurs at the particle's outer surface, forming a PDA shell while leaving a substantial fraction of PCDA unpolymerized in the interior due to limited UV penetration [37]. This internal PCDA reservoir can migrate, redistribute, or form voids in the presence of PCDA-solubilizing solvents, thereby coupling molecular transport to the observed chromatic response.

Despite prior observations of thermally induced blue-to-red transitions in PDA particles [30, 38], the effects of unpolymerized PCDA, the impact of PCDA melting, and the mechanisms underlying semi-reversible thermochromism have yet to be systematically investigated. Given that PCDA melts at ~ 64 °C (Fig. S1), we hypothesize that heating above the melting point induces not only liquefaction of internal PCDA (Fig. 1b) but also mobilization of PCDA trapped between polymerized outer layers (Fig. 1c). This migration and structural rearrangement can deform the PDA backbone, contributing to the thermochromic transition in addition to direct thermal perturbation of the conjugated structure. In PDA–polymer hybrid systems, the surrounding matrix can strongly influence these processes. In particular, PDMS provides optical transparency, flexibility, and relatively high permeability [36, 39], which can facilitate the mobility and redistribution of molten PCDA during thermal cycling.

In this study, we constructed four PDA–PDMS hybrid model architectures that isolate the effects of geometry, confinement, and PCDA reservoir distribution: (i) core–shell PDA@PDMS particles, each containing a single micrometer-sized PDA core ($d \approx 50$–200 μm) encapsulated within PDMS; (ii) nested-PDAs|PDMS particles, in which multiple submicrometer- to micrometer-scale PDA particles ($d \lesssim 10$ μm) are embedded within PDMS; (iii) PDA/PDMS composite particles, prepared by blending PCDA with PDMS followed by solvent-evaporation and UV polymerization to distribute PDA throughout the PDMS matrix; and (iv) PDA|PDMS laminates, in which a PDA film is embedded in a PDMS layer. These model systems allow direct evaluation of the hypothesis that heating above the PCDA melting point induces PCDA liquefaction and migration, followed by local reassembly of PCDA into ordered structures that subsequently undergo UV-induced polymerization to form new blue-phase PDA domains (Fig. 1d). These sequential processes collectively govern the thermochromic trajectory, hysteresis, and degree of semi-reversible recovery. By systematically comparing chromatic responses across architectures, this work clarifies how confinement, interfacial area, and PCDA mobility within PDMS dictate semi-reversible thermochromism, and establishes a materials-level framework for designing thermochromic systems with tunable thermal-memory characteristics relevant to optical temperature indicators and thermal-history sensing platforms.

2 Experimental section

2.1 Fabrication of microfluidic devices

Micrometer-scale PDA particles (50–200 μm in diameter) were produced using a custom glass-capillary microfluidic device (device 1, Fig. 2a). Core–shell PDA@PDMS particles, nested-PDAs|PDMS particles, and PDA/PDMS composite particles were generated using a similar setup (device 2, Fig. 2b). All devices were assembled in a coaxial capillary configuration mounted on a glass slide. A circular glass capillary (CC-1; length 50 mm, I.D. = 0.58 mm, O.D. = 1.0 mm; World Precision Instruments, USA) was first tapered using a micropipette puller (Model P-1000, Sutter Instrument, USA) and then trimmed with a microforge (MF-830, Narishige, Japan) to produce nozzle openings of controlled diameter. For device 1, the nozzle diameter was adjusted according to the target PDA particle size, with typical orifice diameters of approximately 10, 20, and 40 μm used to fabricate PDA particles with diameters of ~ 50, 100, and 200 μm, respectively. For device 2, the nozzle opening of CC-1 was enlarged to roughly 240 μm by gentle polishing with fine sandpaper to accommodate the generation of larger droplets. To render the inner wall of CC-1 hydrophobic for device 1, a 10 vol% solution of OTS in toluene was introduced and the capillary was heated at 140 °C for 1 h. The CC-1 used in device 2 was left uncoated. A square capillary (SC; I.D. = 1.05 mm, 20 mm length; AIT Glass, USA) was fixed on a glass slide (52 × 76 mm, Matsunami, Japan). The prepared CC-1 was inserted into one end of the SC, and a second circular capillary (CC-2, 50 mm) was inserted from the opposite side until the tip of CC-1 extended slightly into CC-2. The outer end of CC-2 was gently heated and bent downward to guide the formed droplets into a collection vessel. A stainless-steel dispensing needle (20 G, Weller, Germany) was attached to the side gap between the SC and CC-1 to introduce the continuous phase. All junctions were sealed with fast-curing epoxy (Devcon, USA) and allowed to harden for approximately 12 h at ambient temperature.

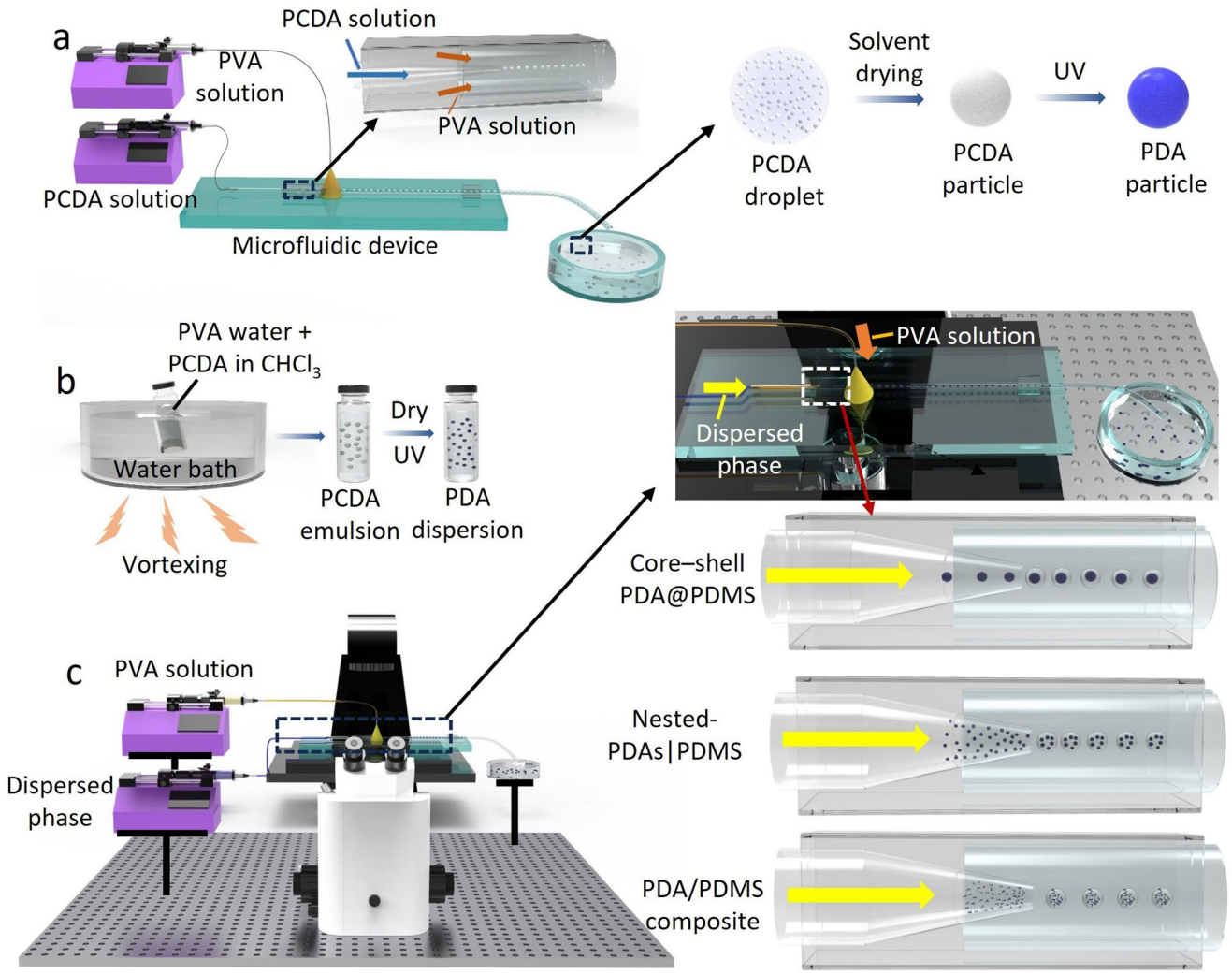


Fig. 2 Fabrication methods of PDA–PDMS hybrid particles. **a** Formation of micrometer-sized PDA particles ($d \approx 50$–200 μm) using a flow-focusing microfluidic method. **b** Preparation of submicrometer- to micrometer-scale PDA particles ($d \lesssim 10$ μm) via an emulsification method. **c** Fabrication of PDA–PDMS particles by varying the inner-phase feed: core–shell PDA@PDMS particles, nested-PDAs|PDMS particles, and PDA/PDMS composite particles

2.2 Fabrication of micrometer-sized PDA particles

The micrometer-sized PDA particles were produced using microfluidic device 1 (Fig. 2a) [30, 40]. A dispersed phase composed of 10 wt% PCDA monomers dissolved in chloroform was introduced into CC-1 through a syringe pump (Pump 11 Elite, Harvard Apparatus, USA). Before injection, the PCDA–chloroform mixture was filtered through a 0.45 μm polytetrafluoroethylene (PTFE) syringe filter (Whatman, USA). A 2 wt% aqueous PVA solution was used as the continuous phase and supplied to the needle port between the SC and CC-1 using a second syringe pump. During droplet generation, the PVA solution acted as a stabilizing medium for the PCDA-chloroform droplets. The dispersed-phase flow rate was fixed at 5 $\mu L \cdot min^{-1}$, while the continuous-phase flow rate was adjusted according to the target PDA particle size. Specifically, flow rates of 350, 650, and 2000 $\mu L \cdot min^{-1}$ were used to produce PDA particles with diameters of approximately 200, 100, and 50 μm, respectively. These conditions ensured stable and uniform generation of PCDA–chloroform droplets. The droplets emerging from CC-2 were collected in a water-filled glass Petri dish and left undisturbed overnight at room temperature in the dark, allowing the solvent to evaporate and solid PCDA particles to form. The resulting solid PCDA particles suspended in water were subsequently polymerized under 254 nm UV irradiation to form PDA (1 W; VL-6LC, Vilber Lourmat, France) at a power density of 0.4 $mW \cdot cm^{-2}$. Unless otherwise specified, UV exposure was applied for 10 min, followed by gentle manual agitation. This procedure was repeated five additional times to ensure homogeneous exposure. The

resulting PDA particles were washed three times with deionized ultrapure water (DIW) to remove excess PVA and then stored in fresh water until use.

2.3 Fabrication of submicrometer- to micrometer-scale PDA particles

Submicrometer- to micrometer-scale PDA particles were prepared through an emulsification-based approach (Fig. 2b) [34]. A 10 wt% solution of PCDA in chloroform was filtered through a 0.2 μm PTFE syringe filter (LK LAB, Korea) prior to use. 1 mL of the PCDA solution was added to 10 mL of DIW containing 2 wt% PVA. The resulting mixture was vortexed at 3000 rpm for 15 min using a vortex mixer (Scilogex, USA) to generate a stable dispersion of PCDA droplets in the aqueous phase. The emulsion was allowed to stand for 24 h. Afterward, 200 μL of the lower PCDA-rich phase was collected and transferred into a Petri dish containing 50 mL of DIW. The dispersion was left under ambient conditions for three days to allow chloroform evaporation and formation of solid PCDA particles. Polymerization of the PCDA particles was performed by UV irradiation (254 nm) for a total duration of 15 min, divided into two 7.5 min exposures separated by a 30 s period of gentle agitation. Residual PVA was removed by five sequential centrifugation-redispersion cycles with DIW. The resulting PDA particles were finally redispersed and stored in fresh water until use.

2.4 Fabrication of PDA–PDMS hybrid particles

Three types of PDA–PDMS hybrid particles (i.e., core–shell PDA@PDMS, nested-PDAs|PDMS, and PDA/PDMS particles) were produced using microfluidic device 2 (Fig. 2c). A 2 wt% PVA aqueous solution was used as the continuous phase and introduced through the needle port into the gap between the SC and CC-1 at a flow rate of 30 mL·h^{-1}. For the dispersed phase of core–shell PDA@PDMS and nested-PDAs|PDMS particles, micrometer-sized PDA particles ($d \approx 50$–200 μm) or submicrometer- to micrometer-scale PDA particles ($d \lesssim 10$ μm), respectively, were suspended in 2.0 g of PDMS premixed with 0.2 g of curing agent. This dispersion was injected into CC-1 at 0.2 mL·h^{-1}. The resulting PDMS droplets containing PDA particles were collected in a water-filled glass Petri dish and kept in the dark at room temperature for approximately 3 days to allow complete PDMS curing. The cured core–shell PDA@PDMS and nested-PDAs|PDMS particles were then washed three times with DIW and stored in fresh water at room temperature until use.

For PDA/PDMS composite particles, the dispersed phase was prepared by dissolving 0.163 g of PCDA monomers in 1 mL of chloroform and mixing this solution with 10 g of PDMS containing 1 g of curing agent. The mixture was injected into CC-1 under the same flow conditions as above. The droplets were collected in a water-filled Petri dish and cured in the dark at room temperature for about 3 days. The solidified PCDA/PDMS composite particles were subsequently photopolymerized under 254 nm UV irradiation for 15 min while the suspension was gently agitated to ensure uniform exposure. Finally, the resulting PDA/PDMS composite particles were rinsed three times with DIW and stored in fresh water in the dark until further experiments.

2.5 Preparation of PDA|PDMS laminates

A 15 wt% PCDA solution was prepared by dissolving 2.36 g of PCDA in 10 mL of chloroform, followed by filtration through a PTFE syringe filter. A 200 μL aliquot of the filtered solution was spin-coated onto a cover glass (22 × 22 mm, BRAND, Germany) at 700 rpm using a spin coater (Spin-1200D, MIDAS SYSTEM Co., Ltd., South Korea). The resulting PCDA-coated film was exposed to UV light (254 nm) to polymerize the monomers into PDA with different UV exposure times (t_{UV} = 1, 3, or 6 min). To fabricate PDA|PDMS laminates with PDMS layer thicknesses of approximately 2, 4, and 6 mm, hollow square molds (75 × 75 mm) were designed using Rhino software and printed with a 3D printer (UltiMaker S5, Netherlands) using PLA filament (Ø 2.85 mm, UltiMaker, Netherlands). The molds were fixed onto a square dish (125 × 125 × 20 mm, SPL Life Sciences, South Korea) with UV-curable epoxy (NOA81, Norland Products Inc., USA). PDA-coated cover glasses with different t_{UV} values were placed inside the molds, and PDMS (Sylgard 184 A and 184B mixed at a 10:1 ratio) was poured into each mold until the desired PDMS layer thickness was reached. The samples were left at room temperature in the dark for two days to allow natural curing of the PDMS. After curing, the PDA|PDMS laminates were carefully removed from the molds and trimmed with a clean blade to obtain laminates with final PDMS thicknesses of ~2, 4, and 6 mm. PDA films prepared with different UV polymerization times (t_{UV} = 1, 3, and 6 min) were independently used for subsequent experiments.

3 Results and discussion

3.1 Preparation and characterization of PDA–PDMS hybrid particles

Figure 3 summarizes the optical and morphological characteristics of the PDA particles and the PDA–PDMS hybrid particles used in this study. Monodisperse PDA microparticles with diameters of approximately 50, 100, and 200 μm were successfully generated by microfluidics, as shown in the bright-field images (Fig. 3a). SEM analysis (Fig. 3b) revealed

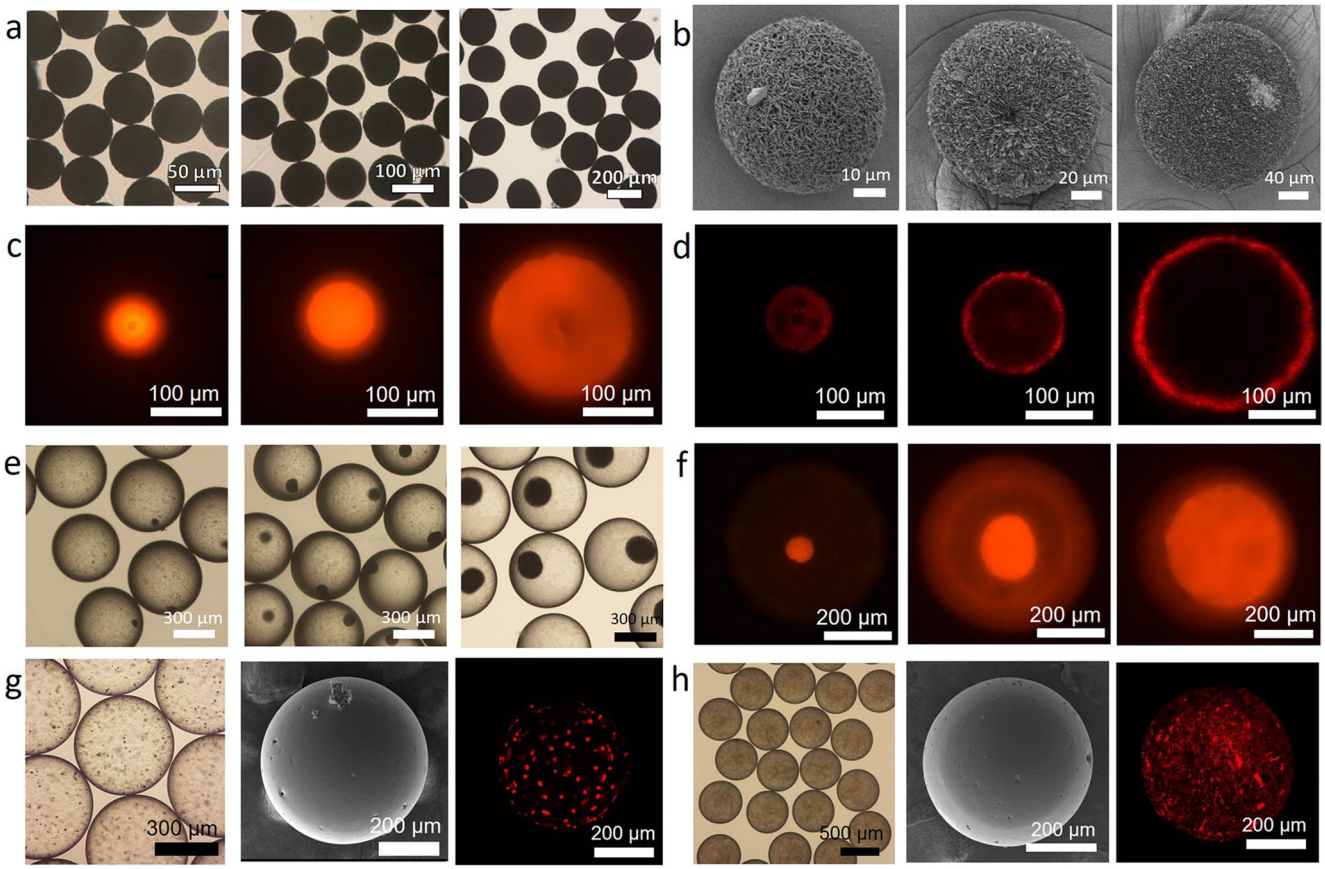


Fig. 3 Characterization of PDA–PDMS particles. **a, b** Bright-field images of micrometer-sized PDA particles with controlled diameters ($d \approx 50$, 100, and 200 μm) fabricated by the microfluidic method (**a**) and corresponding SEM images showing their surface morphology (**b**). **c** Fluorescence microscopy images of heat-treated PDA microparticles of different diameters, exhibiting red-phase emission. **d** Confocal images of the heat-treated PDA microparticles showing red fluorescence localized near the outer region. **e**, **f** Bright-field images of core–shell PDA@PDMS particles with varying PDA core diameters (**e**) and corresponding fluorescence images after heat treatment (**f**). **g** Bright-field, SEM, and confocal images of nested-PDAs|PDMS particles. **h** Bright-field, SEM, and confocal images of PDA/PDMS composite particles. Heat treatment was performed at 100 °C for 3 min

that the PDA microparticles exhibit a rough, flake-like surface morphology composed of densely packed platelet structures, characteristic of the polymerized PDA layer [30]. Upon heating, all PDA microparticles exhibited a uniform blue-to-red chromatic transition accompanied by a strong red-phase fluorescence emission (Fig. 3c). Confocal imaging confirmed that the heat-activated fluorescence is concentrated at the particle periphery (Fig. 3d), consistent with the expected formation of a predominantly polymerized outer layer resulting from limited UV penetration during photopolymerization [37].

Embedding PDA within PDMS resulted in three distinct hybrid structures: core–shell PDA@PDMS particles, nested-PDAs|PDMS particles, and PDA/PDMS composite particles. In the core–shell PDA@PDMS particles, a single PDA microparticle is encapsulated within PDMS; bright-field and fluorescence images (Fig. 3e, f) show that the PDA core remains intact and capable of thermally active fluorescence. The nested-PDAs|PDMS particles (Fig. 3g), which contain multiple submicrometer- to micrometer-scale PDA particles embedded within the PDMS matrix, exhibit a dispersed arrangement in bright-field images and, after heating, show distinct red-emission spots corresponding to individual PDA domains. The PDA/PDMS composite particles (Fig. 3h) exhibit irregularly dispersed PDA domains that vary in size and frequently form local clusters throughout the PDMS matrix, resulting in a clustered fluorescence pattern upon heat-induced activation. Together, these observations demonstrate that the fabrication approaches reliably produce well-defined PDA–PDMS hybrid architectures with controlled structural organization, establishing a robust platform for investigating heat-driven chromatic transitions and semi-reversible behavior.

3.2 Raman spectroscopy analysis

Raman spectroscopy was used to further elucidate the molecular origins of the thermochromic transitions observed in PDA and PDA–PDMS architectures (Fig. 4). As shown in Fig. 4a, a single PCDA particle exhibits a prominent Raman

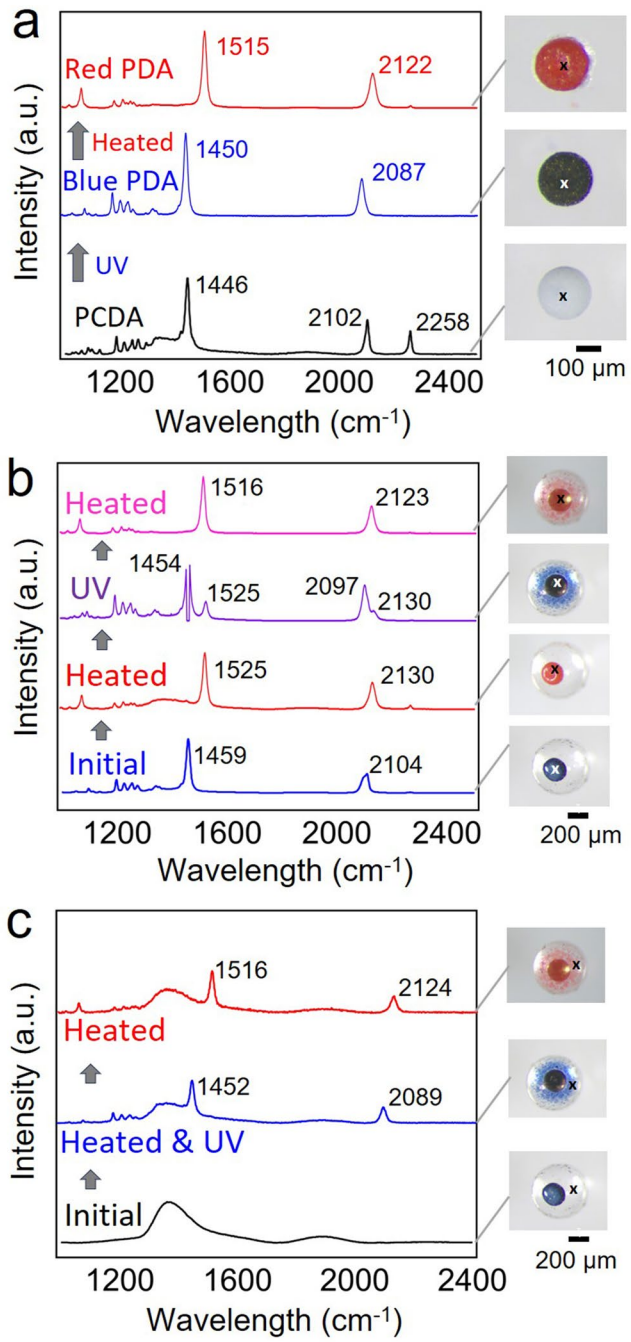


Fig. 4 Raman spectroscopic analysis of PDA and core–shell PDA@PDMS particles. **a** Raman spectra of PCDA, blue-phase PDA, and heat-treated red-phase PDA particles ($d \approx 200$ μm). **b**, **c** Raman spectra collected from the core (**b**) and shell (**c**) regions of PDA@PDMS particles with a 200 μm PDA core, measured at successive stages: initial state, after heating, after UV irradiation, and after reheating. The × marks indicate the positions where the Raman confocal laser was focused

band at ~ 2258 cm^{-1}, which is assigned to the C ≡ C stretching mode of the diacetylene monomer [41, 42]. In addition, the bands at ~ 2102 and 1446 cm^{-1} were observed, which are attributed to a trace amount of PDA formed by unintended polymerization during Raman measurement, consistent with previous reports [36, 38, 43, 44]. Even when only a small amount of PDA is present in a predominantly PCDA sample, PDA-related Raman bands can appear relatively prominent because the conjugated PDA backbone exhibits strong Raman activity and resonance Raman enhancement. Following intentional UV photopolymerization, the Raman spectrum of blue-phase PDA is characterized by bands at ~ 2087 and 1450 cm^{-1}, reflecting the formation of an extended conjugated ene–yne backbone. Upon subsequent heating, these bands shift to ~ 2122 and 1515 cm^{-1}, respectively, indicating a reduction in effective π-conjugation and backbone distortion associated with the blue-to-red transition.

To examine how the thermochromic transition evolves within a PDA@PDMS particle, Raman spectra were collected separately from the PDA core (Fig. 4b) and the surrounding PDMS shell (Fig. 4c). In the core region (Fig. 4b), the initial spectrum displays characteristic bands of blue-phase PDA at ~2104 and 1459 cm^{-1}. Upon heating, these bands shift to ~2130 and 1525 cm^{-1}, consistent with the formation of the red-phase. Subsequent UV irradiation partially restores blue-phase features at ~2097 and 1454 cm^{-1}, indicating the generation of newly polymerized PDA domains. A following heating step again induces the typical blue-to-red peak shift (~2123 and 1516 cm^{-1}), confirming the semi-reversible thermochromic behavior of the PDA core. In contrast, the PDMS shell initially exhibits no detectable PCDA- or PDA-related Raman features (Fig. 4c). After heating and UV irradiation, blue-phase PDA bands emerge in the shell at ~2089 and 1452 cm^{-1}, consistent with polymerization of PCDA that migrated outward from the core into the PDMS matrix. Subsequent heating then induces a red-phase transition of these newly formed PDA domains, as evidenced by peak shifts to ~2124 and 1516 cm^{-1}.

Taken together, the Raman results support a mechanistic picture in which PCDA melting, outward migration, and UV-induced polymerization play central roles in the semi-reversible chromatic behavior. The spectra reveal that limited UV penetration produces a PDA outer layer surrounding a PCDA-rich interior, and that heat-induced PCDA mobility, followed by localized polymerization within the PDMS matrix, generates new PDA domains that give rise to the observed semi-reversibility.

3.3 Semi-reversibility of PDA–PDMS hybrid particles

Figure 5 summarizes the semi-reversible thermochromic behavior of core–shell PDA@PDMS particles containing a ~200 μm PDA core. Figure 5a and b show polarized-microscope images collected over four heating–cooling cycles at 80, 100, and 120 °C, performed either with (a) or

without (b) a 3 min UV-irradiation step. Under UV-assisted cycling (Fig. 5a), the PDA core undergoes a clear blue-to-red transition during heating at 100 and 120 °C and partially returns toward the blue state after cooling and UV exposure, demonstrating semi-reversibility. At 80 °C, however, color changes in the core are minimal, indicating that this condition is insufficient to induce substantial PCDA mobilization. While minor backbone distortion may still occur at 80 °C, its effect is weak and does not lead to pronounced chromatic transitions or effective recovery. In contrast, the stronger recovery observed at higher temperatures reflects enhanced PCDA mobility combined with more pronounced PDA backbone distortion under elevated thermal conditions, which together facilitate semi-reversible behavior.

Notably, the PDMS shell also undergoes characteristic color changes once the first heating–cooling–UV sequence is completed (Fig. 5a). After the first cycle, a blue hue appears in the shell, which is attributed to unpolymerized PCDA eluting from the PDA core, diffusing into the PDMS matrix, and subsequently polymerizing under UV exposure. As the cycles proceed, the shell exhibits a clear sequence of chromatic transitions: during the second cycle, the shell shifts from red to a purple tone; during the third cycle, the color deepens from red to magenta-like color; and similar transitions occur in the subsequent cycle. These color change patterns become more pronounced at higher temperatures. The accompanying reflected-light stereoscope images (insets in Fig. 5a) show the corresponding macroscopic appearance observable by the naked eye.

In the absence of UV irradiation (Fig. 5b), the PDA core remains in the red state after repeated heating–cooling cycles, showing minimal recovery and indicating that UV-induced polymerization is required to generate new blue-phase PDA domains and maintain semi-reversible thermochromism. Under these conditions, bright whitish regions appear within the PDMS shell after heating and cooling, as observed in Fig. 5b and more clearly in the magnified polarized-microscope images shown in Fig. S2 for the 120 °C case. Similar bright regions are also detected at 100 and 80 °C, although their extent is noticeably smaller at lower temperatures. Importantly, the amount and spatial coverage of these bright domains increase progressively with repeated thermal cycling. Upon reheating, these regions diminish as PCDA redissolves, while subsequent cooling leads to their reappearance, consistent with temperature-dependent crystallization or self-assembly of PCDA that has migrated into the PDMS matrix. The accumulation of these bright domains with cycling provides additional evidence that heating induces PCDA elution from the PDA core and its gradual redistribution and organization within the PDMS shell.

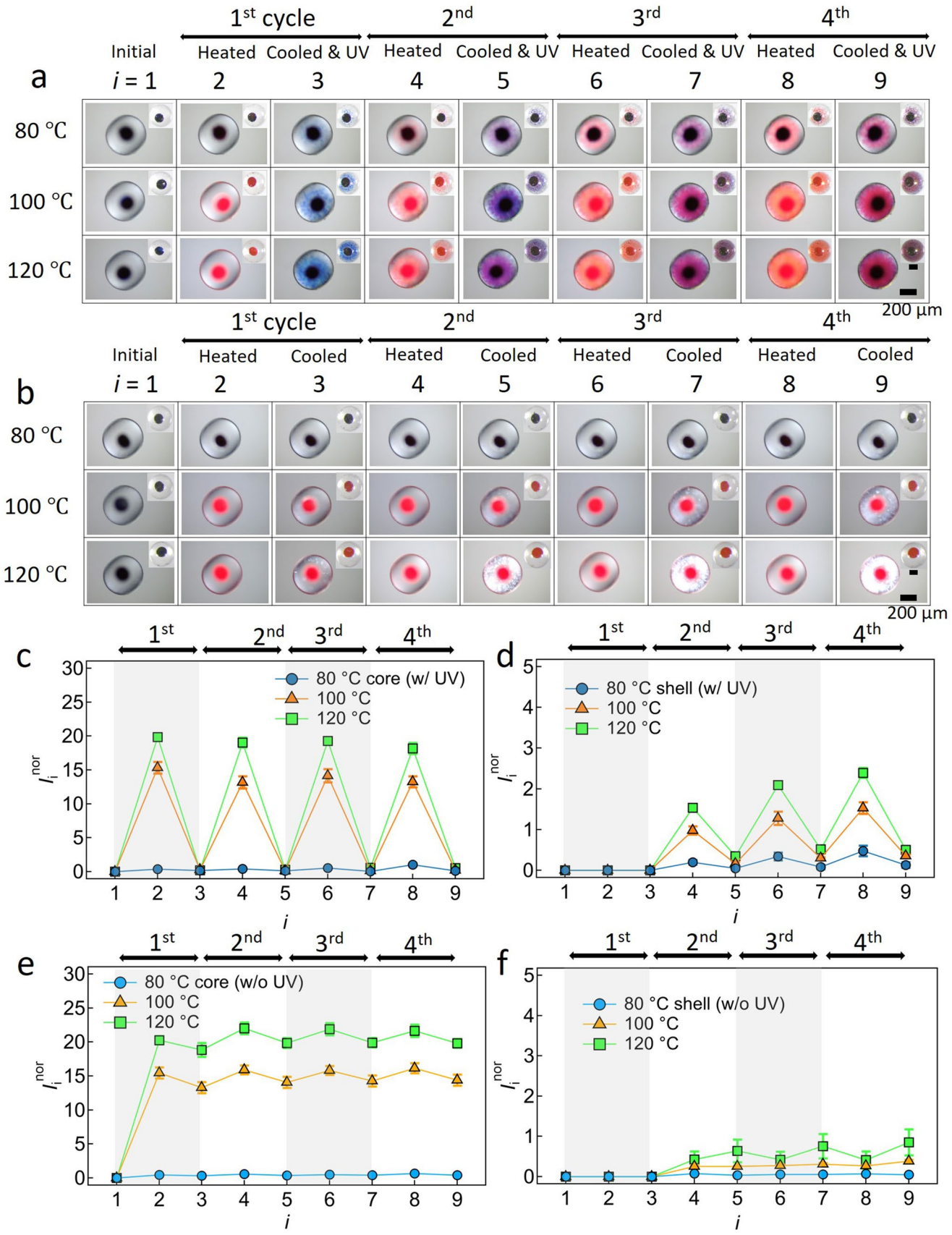
Fig. 5 Semi-reversible thermochromic response of core–shell PDA@PDMS particles (PDA core≈200 μm). **a, b** Polarized optical microscope images recorded over four thermal cycles consisting of heating to 80, 100, or 120 °C and cooling to 27 °C, with (**a**) and without (**b**) a 3-min UV irradiation step. Insets show the corresponding reflected-light stereomicroscope images. All scale bars are 200 μm. **c**–**f** Normalized mean red intensity (I_i^{nor}) of the PDA core (**c**, **e**) and PDMS shell (**d**, **f**) at 80, 100, and 120 °C across four thermal cycles; panels (**c**, **d**) include UV irradiation, whereas panels (**e, f**) omit it. Error bars represent the standard deviation from measurements of at least three PDA@PDMS particles

Figures 5c–f quantify these observations. For the PDA core (Fig. 5c), repeated cycles with UV exposure yield a distinct zig-zag pattern in the normalized red intensity, reflecting reversible red-phase formation upon heating and partial restoration after UV irradiation. This semi-reversible response is most pronounced at 100 and 120 °C, whereas the core exhibits only a minimal response at 80 °C. In the PDMS shell (Fig. 5d), a weaker yet noticeable semi-reversible behavior emerges at 100 and 120 °C, consistent with PCDA diffusion into the PDMS layer and UV-induced formation of new blue-phase PDA domains.

In the absence of UV irradiation, the PDA core shows an increase in red intensity during the first heating cycle at 100 and 120 °C (Fig. 5e), similar to the UV-assisted case in Fig. 5c. However, unlike the UV-assisted cycles, this initial color change is followed by little or no recovery in subsequent cycles, indicating a loss of reversibility. The weak zig-zag features occasionally observed at 100 and 120 °C are likely attributable to minor, unintended polymerization by ambient illumination during imaging. At 80 °C, the core exhibits negligible color change. The PDMS shell displays almost no blue or red coloration under the UV-omitted conditions (Fig. 5f), confirming that little or no new PDA formation occurs within the shell. These observations collectively indicate that elevated temperatures facilitate PCDA elution from the PDA core into the PDMS matrix, but without UV exposure, the system lacks the means to polymerize the migrated PCDA into new blue-phase PDA domains, leading to predominantly irreversible behavior.

Taken together, the results in Fig. 5 show that semi-reversible thermochromism in PDA@PDMS particles arises from the coupled processes of PCDA melting during heating, partial outward migration of PCDA into the PDMS layer, and UV-assisted polymerization that generates new blue-phase PDA domains. The clear contrast between UV-assisted and UV-omitted cycling demonstrates that UV-induced polymerization of heat-mobilized PCDA is essential for maintaining cycle-to-cycle reversibility.

The thermochromic responses of the other PDA–PDMS architectures under repeated heating–cooling–UV cycles exhibit clear differences depending on the amount and distribution of unpolymerized PCDA (Figs. 6a-c).


a
1st cycle
2nd
3rd
4th
Initial
Heated
Cooled & UV
i = 1
80 °C
100 °C
120 °C
200 μm
b
Cooled
c
80 °C core (w/ UV)
d
80 °C shell (w/ UV)
e
80 °C core (w/o UV)
f
80 °C shell (w/o UV)
i

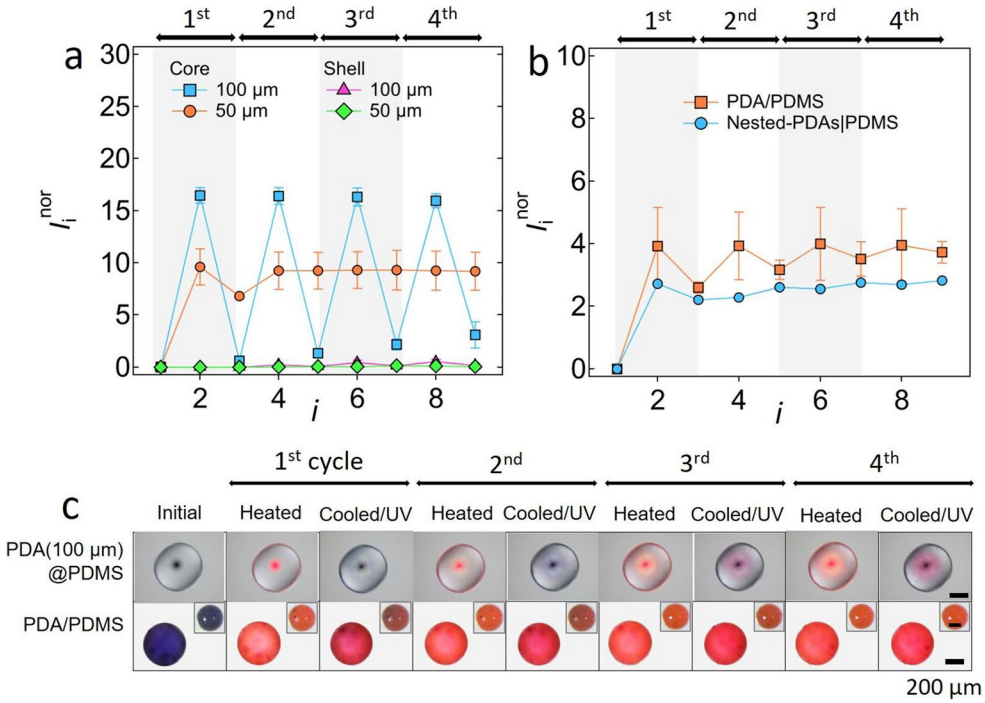


Fig. 6 Thermochromic response in PDA–PDMS hybrid particles. **a** Normalized mean red-channel intensity (I_i^{nor}) for core–shell PDA@PDMS particles measured in the PDA core and PDMS shell with PDA-core diameters of 50 and 100 μm. **b** I_i^{nor} values for PDA/PDMS composite particles and nested-PDAs|PDMS particles. All data represent four thermal cycles consisting of heating to 100 °C, cooling to 27 °C, and a 3-min UV irradiation step included in each cycle. Error bars represent the standard deviation from measurements of at least three PDA–PDMS particles. **c** Example polarized-microscope images of some PDA–PDMS architectures during the heating–cooling–UV cycle. All scale bars are 200 μm

In the core–shell particles with PDA cores of ~100 μm and ~50 μm, the magnitude of the core response strongly depends on the core size (Fig. 6a). The ~100 μm core displays a pronounced semi-reversible zig-zag pattern in normalized red intensity at 100 °C—behavior consistent with the larger 200 μm cores shown in Fig. 5c—whereas the ~50 μm core shows almost no recovery after the initial transition to the red-phase. The PDMS shells in both cases exhibit only minimal color changes and very weak reversibility (Fig. 6a), again in contrast to particles with larger PDA cores. These size-dependent trends reflect the greater reservoir of unpolymerized PCDA in larger cores, which supplies more material capable of melting, migrating, and polymerizing to generate new blue-phase PDA during each cycle.

In PDA/PDMS composite particles, the semi-reversible response is substantially reduced (Fig. 6b). This can be traced to the relatively small amount of unpolymerized PCDA present within the PDMS matrix, which limits both PCDA mobility during heating and the formation of new PDA domains upon UV exposure. A similar outcome is observed for nested-PDAs|PDMS particles (Fig. 6b): although they contain multiple embedded PDA particles, each micro- or submicrometer-sized domain holds only a small PCDA reservoir, leading to weak thermochromic recovery.

Overall, the comparative behaviors across these architectures indicate that the degree of semi-reversible thermochromism is dictated primarily by the effective quantity of unpolymerized PCDA available for melting, migration, and UV-induced polymerization. Structures with larger PCDA reservoirs—particularly large PDA cores—exhibit the stronger semi-reversible behavior, whereas those with limited PCDA content show greatly diminished recovery.

3.4 Visualization of molten PCDA mobility in the PDMS shell

To directly visualize how molten PCDA migrates within a PDMS shell, core–shell PCDA@PDMS particles containing a ~200 μm PCDA core particle were examined under varying PDMS curing times (Fig. 7a). When the PDMS shell was lightly cured ($t_{curing} = 6$ or 12 h), heating to 80 °C caused a substantial portion of the PCDA core to melt and spread throughout the PDMS matrix. After cooling and subsequent UV irradiation, the migrated PCDA partially assembled and polymerized into new PDA domains, producing a distinct blue coloration in the shell. During this process, the high-density PCDA region—likely containing partially polymerized PDA at the outer layer—expanded beyond the size of the original core and segregated toward one side of the PDMS shell. Upon reheating, these newly formed PDA regions underwent the characteristic blue-to-red transition, and cooling/UV exposure regenerated some blue-phase domains, consistent with the behavior illustrated in Fig. 7b for the soft-PDMS case.

Increasing the curing time stiffened the PDMS shell and reduced PCDA mobility. For shells cured≥24 h, PCDA spreading at 80 °C was suppressed (Fig. 7a); nevertheless, the presence of PCDA in the shell was confirmed by the

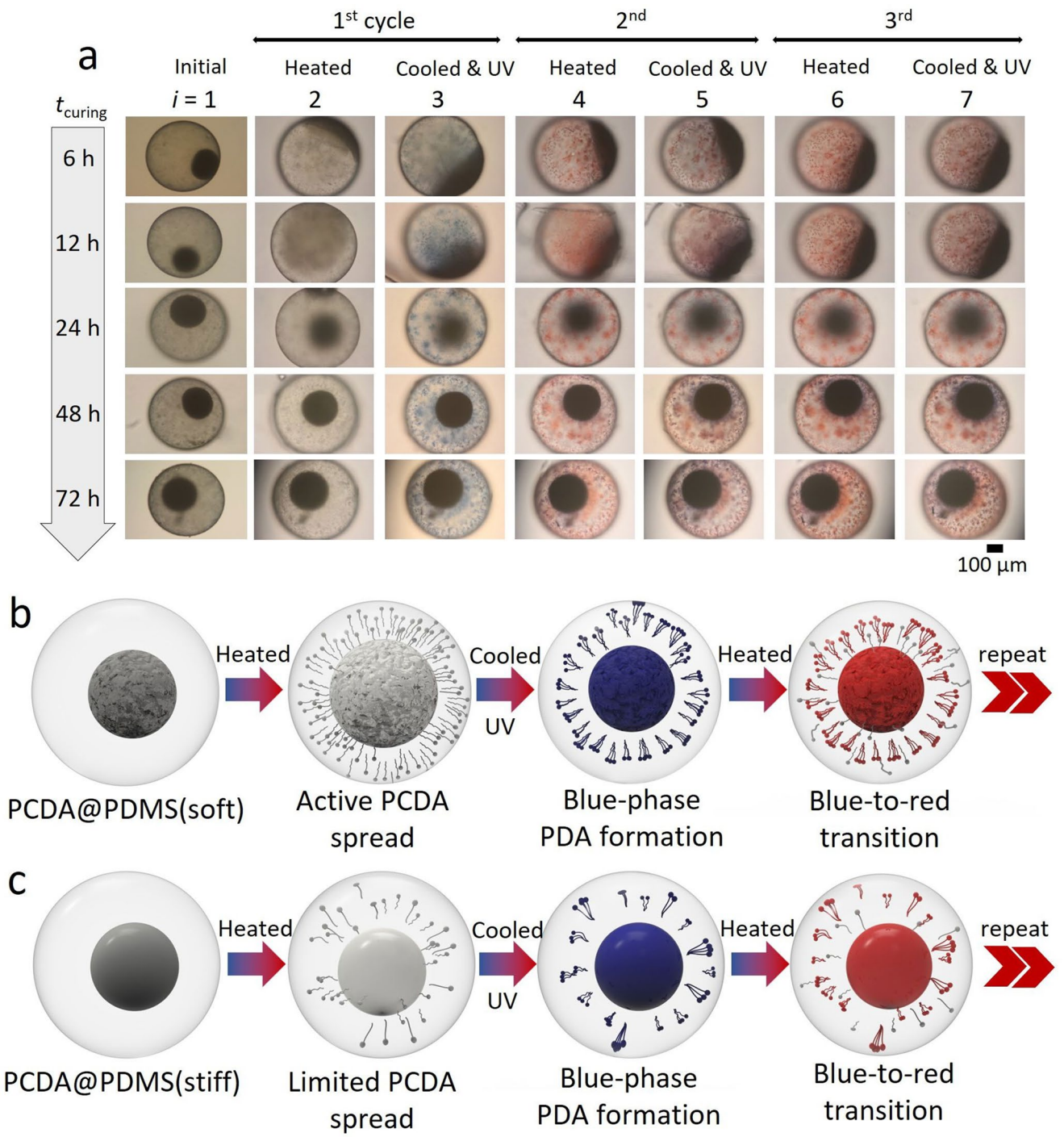


Fig. 7 Thermochromic behavior of core–shell PCDA@PDMS particles with different PDMS stiffness. **a** Optical microscope images showing thermochromic color changes and PCDA migration within PDMS shell during heating at 80 °C, followed by cooling and 3 min of UV irradiation at room temperature, for PCDA@PDMS particles fabricated with varying PDMS curing times (t_{curing}). The heating, cooling, and UV irradiation steps were repeated for three cycles. **b**, **c** Schematic illustration of the process for soft (**b**) and stiff (**c**) PDMS shells corresponding to shorter and longer curing times, followed by PDA formation and color transition through repeated cycles

emergence of newly formed blue-phase PDA following UV irradiation. Repeated heating and cooling/UV cycling produced blue-to-red transitions with observable recovery, but the overall responses remained weaker than in soft-PDMS shells. This trend, schematized in Fig. 7c, reflects restricted transport of PCDA within a highly cross-linked PDMS network, as well as the formation of small PDA domains that nevertheless participate in blue-to-red transitions.

These observations provide mechanistic insight into the results obtained earlier for PDA@PDMS particles with $t_{curing} \geq$ 72 h (Fig. 5), where semi-reversibility was minimal at 80 °C. Although PCDA begins to melt near 64 °C, meaningful thermochromic recovery requires not only melting but also sufficient PCDA mobility for redistribution within and beyond the particle. In the PDA@PDMS system used in Fig. 5, the outer region of the PDA core is already polymerized, which likely acts as a diffusion barrier and hinders the outward migration of molten PCDA at 80 °C. In contrast, the PCDA-core architecture in Fig. 7 permits more direct PCDA melting and spreading into the PDMS shell under similar thermal conditions. At higher temperatures (100–120 °C), PCDA mobility increases substantially, overcoming diffusion constraints and enabling greater migration as well as more extensive UV-induced formation of blue-phase PDA domains.

3.5 Thermochromic behavior of PDA|PDMS laminates

To extend the semi-reversible thermochromic concept beyond particle-based systems, a laminate architecture was constructed by embedding a PDA film within a PDMS layer of controlled thickness. This geometry provides a planar platform that directs heat flow through the PDMS layer and enables direct interrogation of how thermal transport, PCDA mobility, and UV polymerization contribute to chromatic behavior in a confined film-like environment. PDA films were prepared by spin-coating PCDA onto glass substrates, followed by UV polymerization for defined durations (t_{UV} = 1, 3, or 6 min) (Fig. 8a). Owing to the limited penetration depth of UV light, polymerization occurred only in the upper portion of the film, leaving an unpolymerized PCDA layer between the substrate and the PDA layer, as confirmed by

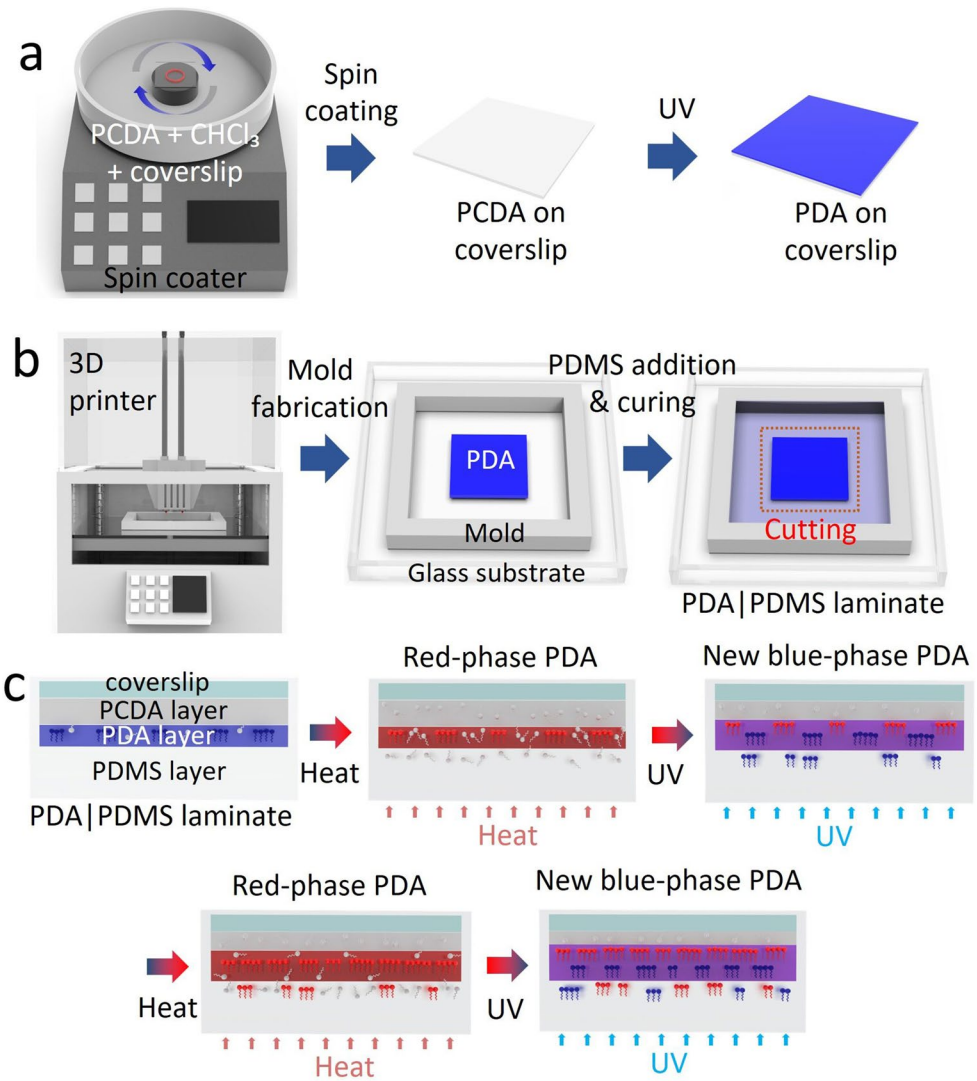


Fig. 8 Fabrication process and proposed semi-reversible thermochromic mechanism of PDA|PDMS laminates. **a**, **b** Schematic illustration of the fabrication process of PDA|PDMS laminates. **c** Proposed mechanism of semi-reversible thermochromism under repeated heating (83 °C) from the PDMS side, cooling, and 3-min UV-irradiation cycles, involving molten PCDA migration and subsequent formation of new blue-phase PDA domains

cross-sectional analysis (Fig. S3). The resulting stratified films were then encapsulated in PDMS layers of varying thicknesses (Fig. 8b).

Upon heating through the PDMS side, the PDA film underwent a blue-to-red transition, consistent with backbone distortion driven by thermal stimulation (Fig. 8c). Cooling followed by 3 min of UV irradiation partially generated new blue-phase PDA domains, and repeating this heating–cooling–UV cycle produced semi-reversible color changes analogous to those observed in particle-based systems (Fig. 5). Figures 9a–c show that the extent and rate of the red-phase development strongly depend on the PDMS layer thickness (h_{PDMS}). Thinner laminates ($h_{\mathrm{PDMS}} \approx 2$ mm; Fig. 9a) heat more rapidly and reach the transition temperature sooner, leading to faster and more pronounced red-phase formation compared to thicker laminates (4 and 6 mm; Figs. 9b, c). In thicker PDMS layers, the delayed temperature rise slows the red-intensity evolution and weakens the semi-reversible response across cycles, highlighting the critical role of heat transfer efficiency in determining thermochromic performance.

The polymerization time of the PDA film further modulates this behavior (Figs. 9a–f). Films prepared with shorter UV exposure ($t_{\mathrm{UV}} = 1$ min) exhibit stronger red-phase development during heating and clearer semi-reversible behavior, whereas films polymerized for longer durations ($t_{\mathrm{UV}} = 3$ or 6 min) show reduced red-intensity development and diminished reversibility. This trend directly correlates with the amount of unpolymerized PCDA remaining in the film. As shown in Fig. S3, increasing t_{UV} systematically increases the thickness of the polymerized PDA layer (h_{PDA}) while decreasing the thickness of the PCDA layer (h_{PCDA}), confirming that shorter UV exposure preserves a larger PCDA reservoir. Consequently, films polymerized for shorter times retain more PCDA available for melting and reorganization during heating, enabling stronger semi-reversible thermochromic responses.

Overall, the laminate results demonstrate that semi-reversibility in PDA-based materials is governed by the interplay between thermal transport (controlled here by PDMS thickness) and the availability of unpolymerized PCDA (regulated by UV polymerization time). By tuning these parameters, the thermochromic trajectory and degree of reversibility can be modulated, suggesting that PDA|PDMS laminates provide a versatile platform for designing film-based thermal indicators with programmable response characteristics.

To facilitate comparison among the four PDA–PDMS architectures investigated in this study, the key structural characteristics, PCDA reservoir size, thermochromic reversibility, and dominant mechanistic features are summarized in Table 1.

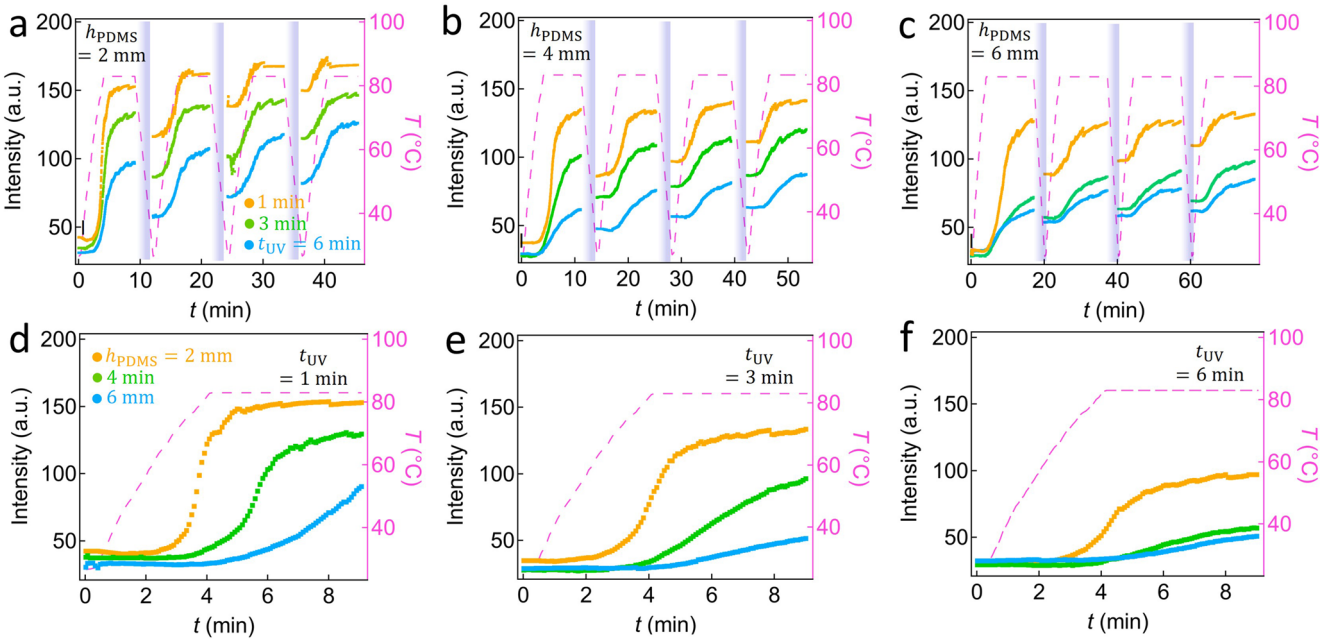


Fig. 9 Semi-reversible thermochromic behavior of PDA|PDMS laminates with different PDMS thicknesses and UV polymerization conditions. **a**–**c** Evolution of red-phase intensity during four repeated heating–cooling–UV irradiation cycles for laminates with PDMS thicknesses of $h_{\mathrm{PDMS}} \approx 2$ mm (**a**), 4 mm (**b**), and 6 mm (**c**). **d**–**f** Red-intensity profiles during the first heating cycle for laminates with PDA films polymerized for $t_{\mathrm{UV}} = 1$ min (**d**), 3 min (**e**), and 6 min (**f**)

Table 1 Comparative summary of the structural characteristics and thermochromic behaviors of the four PDA–PDMS architectures

System	Structure	Characteristic size	PCDA reservoir	Semi-reversibility	Dominant mechanism
Core–shell PDA@PDMS	Single large PDA core encapsulated in PDMS	50–200 μm core	High (core-size-dependent)	Strong (depends on core size)	Molten PCDA migration and UV-induced PDA regeneration
Nested-PDAs|PDMS	Multiple small PDA particles embedded in PDMS	$\lesssim 10$ μm	Low	Weak and limited	Limited PCDA reservoir for regeneration
PDA/PDMS composite	PDA distributed throughout PDMS	Distributed domains	Low	Weak and limited	Limited PCDA reservoir for regeneration
PDA|PDMS laminate	PDA film embedded in PDMS layer	Film geometry	Moderate (PDMS-thickness-dependent)	Moderate and tunable	Molten PCDA migration and UV-induced PDA regeneration

4 Conclusions

In this study, we systematically examined the thermochromic behavior of PDA–PDMS hybrid architectures and identified the key processes underlying their semi-reversible color transitions. By comparing core–shell PDA@PDMS particles, nested-PDAs|PDMS particles, PDA/PDMS composite particles, and PDA|PDMS laminates, we show that semi-reversibility arises from the melting of residual, unpolymerized PCDA, its migration within the PDMS matrix, and subsequent UV-assisted formation of new PDA domains. The strength and reproducibility of the thermochromic response are primarily governed by the available PCDA reservoir and the transport properties of the surrounding PDMS, which together control PCDA mobility during thermal cycling.

These results establish a proof-of-concept mechanistic framework for designing PDA-based thermochromic materials with tunable thermal-memory characteristics and cycle-to-cycle performance. Building on this framework, future studies may explore chemical modification of DA headgroups to tailor intermolecular interactions and chromatic response pathways [12, 45–49]. In addition, strategies for controlled introduction or replenishment of PCDA reservoirs—such as solvent-assisted PCDA infusion or thermal infiltration of molten PCDA—may offer routes to restore PCDA content and prolong semi-reversible functionality. Together, these approaches could further improve the balance between responsiveness, reversibility, and stability. The semi-reversible thermochromic behaviors demonstrated in this study may also provide useful design principles for localized microscale thermal sensing using particle-based systems, as well as visual thermal-history indicators, overheating monitoring materials, and surface-integrated thermochromic platforms based on PDA|PDMS laminate architectures.

Supplementary Information The online version contains supplementary material available at https://doi.org/10.1007/s42114-026-01957-7.

Acknowledgements The research was conducted with the support of the equipment and facilities provided by the ACE Center at Kyung Hee University.

Authors' contributions Inwoong Heo: Investigation, Data curation, Formal analysis. Seung Soo Shin: Investigation, Data curation, Formal analysis. Binglun Tu: Investigation, Data curation. Formal analysis. Boyoung Yoon: Investigation, Data curation. Jong-Man Kim: Conceptualization, Methodology, Supervision, Funding acquisition, Writing – review & editing. Bum Jun Park: Conceptualization, Methodology, Supervision, Funding acquisition, Writing – original draft, Writing – review & editing.

Funding This work was supported by the National Research Foundation (NRF) of Korea (RS-2025-00516792, RS-2024-00406741).

Data availability The authors confirm that the data supporting the findings of this study are available within the article and supplementary materials.

Declarations

Competing interests The authors declare no competing interests.

Open Access This article is licensed under a Creative Commons Attribution 4.0 International License, which permits use, sharing, adaptation, distribution and reproduction in any medium or format, as long as you give appropriate credit to the original author(s) and the source, provide a link to the Creative Commons licence, and indicate if changes were made. The images or other third party material in this article are included in the article's Creative Commons licence, unless indicated otherwise in a credit line to the material. If material is not included in the article's Creative Commons licence and your intended use is not permitted by statutory regulation or exceeds the permitted use, you will need to obtain permission directly from the copyright holder. To view a copy of this licence, visit http://creativecommons.org/licenses/by/4.0/.

References

1. Jaszczak-Kuligowska M, Sąsiadek-Andrzejczak E, Safandowska M, Kozicki M, Madiedo LF, Barburski M et al (2025) Thermochromic textile sensors for temperature measurements. Measurement 257:118698. https://doi.org/10.1016/j.measurement.2025.118698
2. Civan L, Kurama S (2023) Preparation and characterization of intelligent thermochromic fabric coatings for the detection of

fever diseases. Mater Chem Phys 305:127977. https://doi.org/10.1016/j.matchemphys.2023.127977
3. Zhang W, Luan S, Fang Y, Zhu L, Yang Y, Tian M et al (2025) Dynamic reversible thermochromic camouflage smart textiles for temperature visualized personal healthcare and thermal management. Chem Eng J 168746. https://doi.org/10.1016/j.cej.2025.168746
4. He Y, Li W, Han N, Wang J, Zhang X (2019) Facile flexible reversible thermochromic membranes based on micro/nanoencapsulated phase change materials for wearable temperature sensor. Appl Energy 247:615–629. https://doi.org/10.1016/j.apenergy.2019.04.077
5. Nagare SM, Hakami A, Biswas PK, Stefanakos EK, Srinivasan SS (2025) A review of thermochromic materials for coating applications: Production, protection, and degradation of organic thermochromic materials. J Coat Technol Res 22:91–115. https://doi.org/10.1007/s11998-024-00982-9
6. Yu Z, MuYu C, Xu H, Zhao J, Yang G (2023) Recent progress in the design of conjugated polydiacetylenes with reversible thermochromic performance: A review. Polym Chem 14:2266–2290. https://doi.org/10.1039/D3PY00213F
7. Bieniaś K, Wieczorek P, Uchacz T, Fryc A, Kmita A, Feng X et al (2025) Enhancing the reversibility of thermochromism of polydiacetylene-based nanostructures embedded in a natural polymer matrix. J Mater Chem C 13:17300–17312. https://doi.org/10.1039/D5TC01233C
8. Mergu N, Son Y-A (2021) Design and synthesis of polydiacetylenes, and their low temperature irreversible thermochromic properties. Dyes Pigm 184:108839. https://doi.org/10.1016/j.dyepig.2020.108839
9. Lee S, Lee J, Lee M, Cho YK, Baek J, Kim J et al (2014) Construction and molecular understanding of an unprecedented, reversibly thermochromic bis-polydiacetylene. Adv Funct Mater 24:3699–3705. https://doi.org/10.1002/adfm.201304147
10. Khanantong C, Charoenthai N, Wacharasindhu S, Sukwattanasinitt M, Yimkaew W, Traiphol N et al (2020) Achieving reversible thermochromism of bisdiynamide polydiacetylene via self-assembling in selected solvents. Colloids Surf A 603:125225. https://doi.org/10.1016/j.colsurfa.2020.125225
11. Tan J, Liu H, Zhang F, Tian T, Wang C (2025) Dual-responsive reversible colorimetric fabric with highly sensitive thermochromism via π-conjugated polydiacetylene for temperature indicating. J Colloid Interface Sci 139367. https://doi.org/10.1016/j.jcis.2025.139367
12. Qian X, Städler B (2019) Recent developments in polydiacetylene-based sensors. Chem Mat 31:1196–1222. https://doi.org/10.1021/acs.chemmater.8b05185
13. Zhu M, Zhu L (2021) Rational design of diphenyldiacetylene-based fluorescent materials enabling a 365-nm light-initiated topochemical polymerization. Chem Asian J 16:2048–2054. https://doi.org/10.1002/asia.202100468
14. Sun X, Chen T, Huang S, Li L, Peng H (2010) Chromatic polydiacetylene with novel sensitivity. Chem Soc Rev 39:4244–4257. https://doi.org/10.1039/C001151G
15. Das B, Jo S, Zheng J, Chen J, Sugihara K (2022) Recent progress in polydiacetylene mechanochromism. Nanoscale 14:1670–1678. https://doi.org/10.1039/D1NR07129G
16. Wen JT, Roper JM, Tsutsui H (2018) Polydiacetylene supramolecules: Synthesis, characterization, and emerging applications. Ind Eng Chem Res 57:9037–9053. https://doi.org/10.1021/acs.iecr.8b00848
17. Jelinek R, Ritenberg M (2013) Polydiacetylenes–recent molecular advances and applications. RSC Adv 3:21192–21201. https://doi.org/10.1039/C3RA42639D
18. Manikandan R, Shauloff N, Jelinek R (2022) Ultra-low-temperature reversible thermochromism and contactless bacterial sensing by chalcone-functionalized polydiacetylene. J Mater Chem C 10:16265–16272. https://doi.org/10.1039/D2TC03604E
19. Juhasz L, Ortuso RD, Sugihara K (2020) Quantitative and anisotropic mechanochromism of polydiacetylene at nanoscale. Nano Lett 21:543–549. https://doi.org/10.1021/acs.nanolett.0c04027
20. Nakamitsu M, Oyama K, Imai H, Fujii S, Oaki Y (2021) Ultrahigh-sensitive compression-stress sensor using integrated stimuli-responsive materials. Adv Mater 33:2008755. https://doi.org/10.1002/adma.202008755
21. Pham TC, Kim YK, Park JB, Jeon S, Ahn J, Yim Y et al (2019) A selective colorimetric and fluorometric chemosensor based on conjugated polydiacetylenes for cadmium ion detection. ChemPhotoChem 3:1133–1137. https://doi.org/10.1002/cptc.201900165
22. Shin H, Jannah F, Yoo EJ, Kim J-M (2022) A colorimetric and fluorescence turn-on sensor for fe (iii) ion based on imidazole-functionalized polydiacetylene. Sens Actuators B Chem 350:130885. https://doi.org/10.1016/j.snb.2021.130885
23. Siribunbandal P, Osotchan T, Kim Y-H, Jaisutti R (2023) Highly sensitive colorimetric ammonia sensors based on polydiacetylene/zinc oxide nanopellet-embedded pdms films for meat spoilage detection. ACS Appl Polym Mater 5:7786–7794. https://doi.org/10.1021/acsapm.3c00993
24. Weston M, Pham A-H, Tubman J, Gao Y, Tjandra AD, Chandrawati R (2022) Polydiacetylene-based sensors for food applications. Mater Adv 3:4088–4102. https://doi.org/10.1039/D1MA01180D
25. Lee S, Lee J, Kim HN, Kim MH, Yoon J (2012) Thermally reversible polydiacetylenes derived from ethylene oxide-containing bisdiacetylenes. Sens Actuators B Chem 173:419–425. https://doi.org/10.1016/j.snb.2012.07.031
26. Saenjaiban A, Thanakkasaranee S, Jantanasakulwong K, Punyodom W, Lee YS, Singjai P et al (2025) Effect of different metal oxide nanoparticle types on thermochromism of polydiacetylene as time-temperature indicators: Structural form, size, colorimetric sensing. Sens Actuators Phys 386:116352. https://doi.org/10.1016/j.sna.2025.116352
27. Chae S, Lee JP, Kim JM (2016) Mechanically drawable thermochromic and mechanothermochromic polydiacetylene sensors. Adv Funct Mater 26:1769–1776. https://doi.org/10.1002/adfm.201504845
28. Weston M, Tjandra AD, Chandrawati R (2020) Tuning chromatic response, sensitivity, and specificity of polydiacetylene-based sensors. Polym Chem 11:166–183. https://doi.org/10.1039/C9PY00949C
29. Merati AA, Moghimian MH, Yousefzadeh M, Moazeni N (2024) Reversible thermo-chromic polyvinilidyn floride/polydiacetylene/zinc oxide composite nanofibers. J Text Inst 115:2307–2318. https://doi.org/10.1080/00405000.2023.2286809
30. Ahmadi N, Lee J, Godiya CB, Kim J-M, Park BJ (2024) A single-particle mechanofluorescent sensor. Nat Commun 15:6094. https://doi.org/10.1038/s41467-024-50361-6
31. Lee HM, Kim YW, Go EM, Revadekar C, Choi KH, Cho Y et al (2023) Direct measurements of the colloidal debye force. Nat Commun 14:3838
32. Jeong HW, Park JW, Lee HM, Choi KH, Lee SJ, Kim JW et al (2022) Retardation of capillary force between janus particles at the oil–water interface. J Phys Chem Lett 13:10018–10024. https://doi.org/10.1021/acs.jpclett.2c02499
33. Ashkin A, Dziedzic JM, Yamane T (1987) Optical trapping and manipulation of single cells using infrared laser beams. Nature 330:769–771. https://doi.org/10.1038/330769a0
34. Shin SS, Kim DY, Bae K, Kang H, Ha SJ, Patil A et al (2024) Optical laser tweezer-directed single particle solvatochromism of conjugated polydiacetylene. Small Struct 5:2400171. https://doi.org/10.1002/sstr.202400171

35. Ahmadi N, Kim DY, Shin SS, Daradmare S, Kim JM, Park BJ (2024) Gas-shearing microfluidic fabrication of polydiacetylene–alginate colorimetric sensor beads. Small Struct 2400340. https://doi.org/10.1002/sstr.202400340
36. Yoon B, Ahmadi N, Heo I, Shin SS, Kim JM, Park BJ (2025) Single particle semi-reversible solvatochromic sensor. Small 21:2412189. https://doi.org/10.1002/smll.202412189
37. Spagnoli S, Briand E, Vickridge I, Fave J-L, Schott M (2017) Method for determining the polymer content in nonsoluble polydiacetylene films: Application to pentacosadiynoic acid. Langmuir 33:1419–1426. https://doi.org/10.1021/acs.langmuir.6b03147
38. Revadekar CC, Shin SS, Kim JM, Park BJ (2025) Synthesis of janus polydiacetylene sensor particles with thermochromism and solvatochromism properties. Small Struct 6:2400554. https://doi.org/10.1002/sstr.202400554
39. Hong J, Park D-H, Baek S, Song S, Lee CW, Kim J-M (2015) Polydiacetylene-embedded microbeads for colorimetric and volumetric sensing of hydrocarbons. ACS Appl Mater Interfaces 7:8339–8343
40. Kim J-W, Han SH, Choi YH, Hamonangan WM, Oh Y, Kim S-H (2022) Recent advances in the microfluidic production of functional microcapsules by multiple-emulsion templating. Lab Chip 22:2259–2291. https://doi.org/10.1039/D2LC00196A
41. Yoon B, Shin H, Kang E-M, Cho DW, Shin K, Chung H et al (2013) Inkjet-compatible single-component polydiacetylene precursors for thermochromic paper sensors. ACS App Mater Interfaces 5:4527–4535. https://doi.org/10.1021/am303300g
42. Goyal S, Sharma D, Deep A, Kumar K, Sharma AL (2024) Polydiacetylene/poly (vinyl alcohol) composite films as a low-temperature irreversible indicator for drug storage applications. ACS Appl Polym Mater 6:4186–4194. https://doi.org/10.1021/acsapm.4c00136
43. Lim JK, Lee Y, Lee K, Gong M, Joo S-W (2007) Reversible thermochromic change of molecular architecture for a diacetylene derivative 10, 12-pentacosadiynoic acid self-assembled thin films on ag surfaces. Chem Lett 36:1226–1227. https://doi.org/10.1246/cl.2007.1226
44. Saito A, Urai Y, Itoh K (1996) Infrared and resonance raman spectroscopic study on the photopolymerization process of the langmuir– blodgett films of a diacetylene monocarboxylic acid, 10, 12-pentacosadiynoic acid. Langmuir 12:3938–3944. https://doi.org/10.1021/la951503z
45. Fang F, Meng F, Luo L (2020) Recent advances on polydiacetylene-based smart materials for biomedical applications. Mater Chem Front 4:1089–1104. https://doi.org/10.1039/C9QM00788A
46. Ahn DJ, Kim J-M (2008) Fluorogenic polydiacetylene supramolecules: Immobilization, micropatterning, and application to label-free chemosensors. Acc Chem Res 41:805–816. https://doi.org/10.1021/ar7002489
47. Hammond PT, Rubner MF (1995) Synthesis and characterization of new mesogenic diacetylene monomers and their polymers. Macromolecules 28:795–805. https://doi.org/10.1021/ma00108a001
48. Khanantong C, Charoenthai N, Phuangkaew T, Kielar F, Traiphol N, Traiphol R (2018) Phase transition, structure and color-transition behaviors of monocarboxylic diacetylene and polydiacetylene assemblies: The opposite effects of alkyl chain length. Colloids Surf A 553:337–348. https://doi.org/10.1016/j.colsurfa.2018.05.081
49. Liu J, Lam JW, Tang BZ (2009) Acetylenic polymers: Syntheses, structures, and functions. Chem Rev 109:5799–5867. https://doi.org/10.1021/cr900149d

Publisher's note Springer Nature remains neutral with regard to jurisdictional claims in published maps and institutional affiliations.